Synthesis, photophysical properties and theoretical studies of new bis-quinolin curcuminoid BF2-complexes and their decomplexed derivatives

Daniel Insuasty, Lorena Cabrera, Alejandro Ortiz, Braulio Insuasty, Jairo Quiroga, Rodrigo Abonia

PII: S1386-1425(20)30042-1

DOI: https://doi.org/10.1016/j.saa.2020.118065

Reference: SAA 118065

To appear in: *Spectrochimica Acta Part A: Molecular and Biomolecular Spectroscopy*

Received date: 1 November 2019

Revised date: 11 January 2020

Accepted date: 11 January 2020

Please cite this article as: D. Insuasty, L. Cabrera, A. Ortiz, et al., Synthesis, photophysical properties and theoretical studies of new bis-quinolin curcuminoid BF2-complexes and their decomplexed derivatives, *Spectrochimica Acta Part A: Molecular and Biomolecular Spectroscopy*(2018), https://doi.org/10.1016/j.saa.2020.118065

Synthesis, photophysical properties and theoretical studies of new *bis*-quinolin curcuminoid BF_2-complexes and their decomplexed derivatives

Daniel Insuasty [a], Lorena Cabrera [b], Alejandro Ortiz [b,c], Braulio Insuasty [b,c], Jairo Quiroga [b,c], Rodrigo Abonia [b,c]*

[a] *Departamento de Química y Biología, División de Ciencias Básicas, Universidad del Norte, Km 5 vía Puerto Colombia, Barranquilla 081007, Colombia*

[b] *Research Group of Heterocyclic Compounds, Department of Chemistry, Universidad del Valle, A.A. 25360 Cali, Colombia*

[c] *Center for Bioinformatics and Photonics-CIBioFI, Universidad del Valle, Calle 13 No. 100-00, Edificio 320, No. 1069, Cali, Colombia*

* Corresponding author. Tel: +(57)-2-3393248. *E-mail addresses:* rodrigo.abonia@correounivalle.edu.co

GRAPHICAL ABSTRACT:

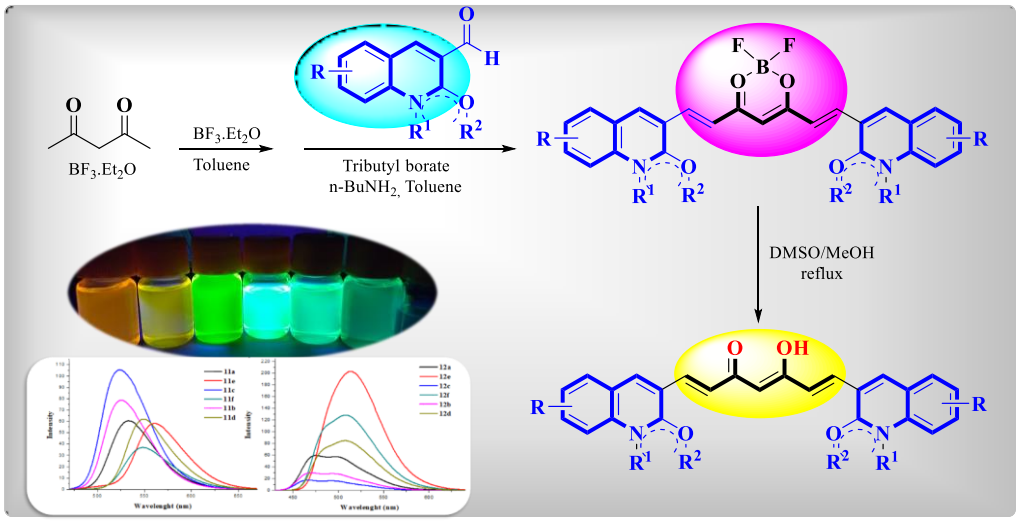

Abstract: This paper presents the synthesis and characterization of two series of new *bis*-quinolin curcuminoid BF_2-

complexes **11** and their respective decomplexed *bis*-quinolin curcuminoid derivatives **12**, in an attempt to understand their optical properties. The synthesized compounds showed interesting fluorescent characteristics in both solution and in solid-state. The characteristic of the electronic transitions involved in these systems were measured via Uv-vis spectroscopy and fluorescence spectroscopy. Results revealed that the absorption and emission bands are dependent of the structure of compounds **11** and **12** but also of the type of substituent, even showing a push-pull behavior in those derivatives substituted with methyl group. These findings were also confirmed through computational calculations at DFT level via simulations of the Uv-vis spectra and determining the topology of the border orbitals responsible for light absorption.

Keywords: Quinolines, Curcumin, absorption spectroscopy, fluorescence spectroscopy, chromophores, BF_2-complexes.

1. Introduction

The last decades there were an increase in the design and synthesis of new organic pigments with outstanding electronic and optical properties [1], due to its broad spectrum of application in the field of nonlinear optics [2], photodynamic therapy [3], organic lasers [4], bioimages [5], organic light-emitting diodes (OLEDs) [6], sensors [7] and photovoltaic [8]. Recently, different curcuminoid derivatives and their boron complexes emerged as an attractive building block for the design of new pigments with enhanced photophysical properties [9–11]. Consequently, different chromophores were used to replace the aryl rings, which acts as electrodonor groups and are directly linked to the enolate [12,13]. For example, previous studies of difluoroboron curcuminoids [14] **1**, showed that an electron-withdrawing substituent in the aromatic ring induced a hypsochromic shift in both emission and absorption bands, while an electrodonor substituent induced a bathochromic shift. Sachin et al. [12] reported the synthesis of difluoroboron *bis*-coumarin analog complexes **2**, in which the quantum fluorescence performance, the absorption, and emission wavelength were sensitive to the polarity of the solvent. This finding was associated with the rigidity of the structure of compounds **2** (thanks to the BF_2-1,3-diketone moiety), and by the electron-withdrawing effect of the BF_2 functionality. Additionally, curcuminoid BF_2-complexes are related with biomedical applications, such as compound **3** that has properties as a bioimage detector [5].

Different study fields also presented an increasing interest in quinolines and their oxo-derivatives due to their numerous practical applications, such as medical and pharmaceutical agents [15,16]. Additionally, quinolines play an important role in optoelectronic applications due to their high thermal and chemical stability, high fluorescence, electron transport, and their possibility of modifications [17–19]. Figure 1 presents some examples of compounds (**4-6**) with optical properties

containing oxo-quinolin fragments in their structures [7,20,21].

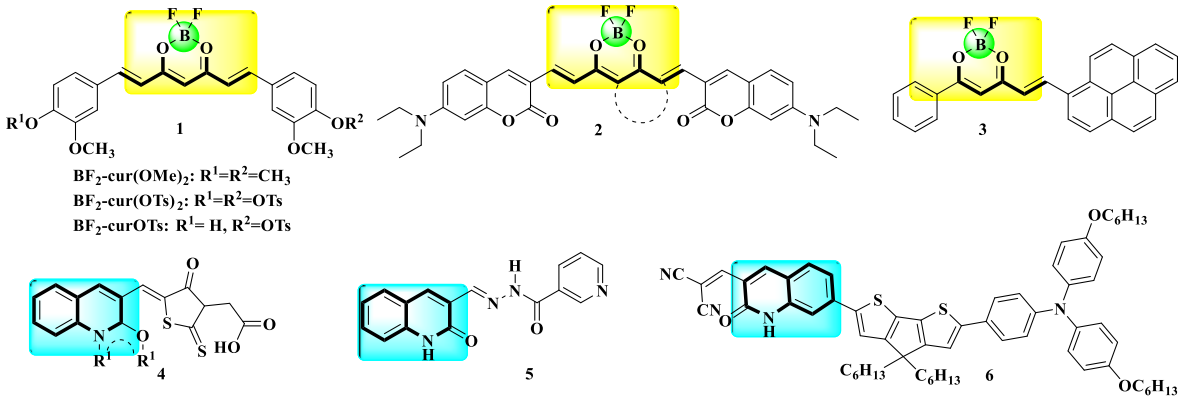

Figure 1. Difluoroboron curcuminoid complexes **1-3** and oxo-quinolin hibrids **4-6** with interesting photophysical and biological properties.

In that scenario, the present study designed, synthesized, and evaluated the absorption and emission properties of new *bis*-quinolin-curcuminoid analogs **11** and **12** containing varied substituted quinolin-moieties as donor fragments and 1,3-diceto (in its enolic form) or 1,3-diketodifluoroborate functionalities as acceptors framed within a push-pull concept (Figure 2). For this study, a set of three *O*-alkyl quinolin- and three *N*-butylquinolone-based structures derived of **11** and their decomplexed analogues **12**, containing an electron donor group (R = CH_3), an electron acceptor group (R = Cl) and a neutral group (R = H) (see Figure 2), was selected, in order to evaluate the behavior of these groups over different photophysical properties. Additionally, the current study presented a solvatochromic study of compounds **11** and **12** in a binary solvent mixture, and a computational analysis using the DFT method.

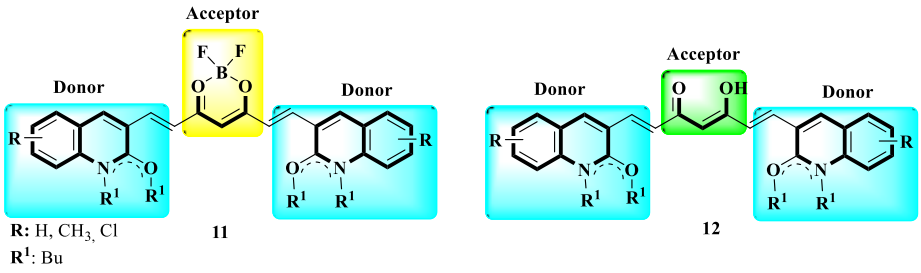

Figure 2. General structure of target molecules **11** and **12**

2. Experimental

2.1. Material and methods

Melting points were measured using a Stuart SMP10 melting point apparatus and are uncorrected. ATR-FTIR spectra were recorded on a Shimadzu IRAffinity–1. 1H and 13C NMR spectra were recorded on a Bruker Avance 400

spectrophotometer operating at 400 MHz and 100 MHz respectively, using DMSO–d_6 and $CDCl_3$ as solvent and tetramethylsilane as internal standard. Chemical shifts are reported in parts per million (ppm) and multiplicities are given as: s (singlet), d (doublet), t (triplet), q (quartet), dd (doublet of doublets), m (multiplet) and the coupling constants *J* are given in Hz. Mass spectra were run on a SHIMADZU-GCMS 2010-DI-2010 spectrometer (equipped with a direct inlet probe) operating at 70 eV. HPLC-HRMS data were obtained on an Agilent Technologies Q-TOF 6520 spectrometer via an electrospray ionization (ESI, 4000 V). UV–Vis absorption spectra of all compounds were recorded on a JASCO V-730 UV–VIS Spectrophotometer. Fluorescence spectra of all the compounds were recorded on a JASCO FP-8500 spectrophotometer. Chemicals and the required solvents were purchased from Sigma-Aldrich, Fluka and Merck (analytical grade reagent), and used without further purification.

2.2. General procedure for the synthesis of the *bis*-quinolin curcuminoid BF_2-complexes 11b-f: A mixture of 2,4-pentanodione (1 equiv.) and $BF_3.Et_2O$ (1.5 equiv.) in toluene (1.5 mL) was heated at 80°C for 2 h. After cooling, a mixture of formylquinolines **10a-f**, (2 equiv.), *N*-butylamine (0.2 equiv.) and tributyl borate (1 equiv.) in toluene was added to the AA-BF_2 solution and was stirred at room temperature for 5 h. The solid formed was filtered and washed repeatedly with toluene, affording pigments **11b-f**.

3.3'-((1E,1'E)-(2,2-Difluoro-2H-1λ^3,3,2λ^4-dioxaborinin-4,6-diyl)bis(etheno-2,1-diyl))bis(2-butoxy-6-methylquinoline)
11b. Orange solid, yield: 94%; m.p. 235-237 °C. FTIR (ATR): ν = 2965 (=C-H), 1602 (C=O), 1508 (C=C) cm^{-1}. ^1H NMR (400 MHz, $CDCl_3$) δ = 1.10 (t, *J* = 7.4 Hz, 6H), 1.57 – 1.66 (m, 4H), 1.92 – 2.00 (m, 4H), 2.53 (s, 6H), 4.61 (t, *J* = 6.7 Hz, 4H), 6.14 (s, 1H), 7.25 (d, *J* = 15.6 Hz, 2H), 7.52 – 7.54 (m, 4H), 7.72 (d, *J* = 9.1 Hz, 2H), 8.15 (s, 2H), 8.22 (d, *J* = 15.6 Hz, 2H). ^{13}C NMR (400 MHz, $CDCl_3$) δ = 14.0, 19.6, 21.3, 31.0, 66.5, 103.2, 119.1, 123.7, 124.8, 126.8, 127.4, 133.8, 134.4, 141.0, 142.5, 145.8, 159.5, 180.4 ppm. ESI-QTOF (positive ionization) M+H calc. for $C_{35}H_{37}BF_2N_2O_4$: 599.2893; found: 599.2888.

3,3'-((1E,1'E)-(2,2-Difluoro-2H-1λ^3,3,2λ^4-dioxaborinin-4,6-diyl)bis(etheno-2,1-diyl))bis(2-butoxyquinoline) **11b**. Orange solid, yield: 75%. m.p. 185-187 °C. FTIR (ATR): ν = 2955 (=C-H), 1624 (C=O), 1518 (C=C) cm^{-1}. ^1H NMR (400 MHz, $CDCl_3$) δ = 1.10 (t, *J* = 7.4 Hz, 6H), 1.56 – 1.66 (m, 4H), 1.91 – 1.98 (m, 4H), 4.60 (t, *J* = 6.7 Hz, 4H), 6.15 (s, 1H), 7.21 – 7.30 (m, 4H), 7.42 (t, *J* = 7.4 Hz, 2H), 7.68 (t, *J* = 7.6 Hz, 2H), 7.75 (d, *J* = 8.1 Hz, 2H), 8.17 – 8.21 (m, 4H). ^{13}C NMR (400 MHz, $CDCl_3$) δ = 14.0, 19.6, 31.0, 66.7, 103.2, 119.3, 123.9, 124.8, 124.8, 127.1, 128.3, 128.4, 131.7, 141.5, 142.3, 159.9, 180.4 ppm. ESI-QTOF (positive ionization) M+H calc. for $C_{33}H_{33}BF_2N_2O_4$: 571.1502; found 571.1508.

3,3'-((1E,1'E)-(2,2-Difluoro-2H-1λ^3,3,2λ^4-dioxaborinin-4,6-diyl)bis(etheno-2,1-diyl))bis(2-butoxy-6-chloroquinoline)
11c. Orange solid, yield: 85%. m.p. 261-263 °C. FTIR (ATR): ν = 2957 (=C-H), 1609 (C=O), 1520 (C=C) cm^{-1}. ^1H NMR (400 MHz, $CDCl_3$) δ = 1.10 (t, *J* = 7.4 Hz, 6H), 1.58 – 1.64 (m, 4H), 1,92 – 2.00 (m, 4H), 4.62 (t, *J* = 6.7 Hz, 4H), 6.16 (s, 1H), 7.25 (d, *J* = 15.7 Hz, 2H), 7.63 (dd, *J* = 8.8, 2.4 Hz, 2H), 7.74 – 7.77 (m, 4H), 8.14 (s, 2H), 8.21 (d, *J* = 15.7 Hz, 2H). NMR (101 MHz, 5) δ = 14.0. 19.6, 31.1, 66.5, 102.7, 106.3, 120.3, 122.5, 125.5, 127.2, 128.2, 135.5, 137.6, 142.2, 156.4, 158.7, 183.5 ppm. ESI-QTOF (positive ionization) M+H calc. for $C_{33}H_{32}BCl_2F_2N_2O_4$: 639.1800; found: 639.1795.

3,3'-((1E,1'E)-(2,2-Difluoro-2H-1λ^3,3,2λ^4-dioxaborinin-4,6-diyl)bis(etheno-2,1-diyl))bis(1-butylquinolin-2(1H)-ona)
11d. red solid, yield: 80%. M.p. 215-217 °C. FTIR (ATR): ν = 2959 (=C-H), 1645 (2 x C=O), 1516 (C=C) cm^{-1}. ^1H NMR (400 MHz, $CDCl_3$) δ = 1.07 (t, *J* = 7.3 Hz, 6H), 1.53 – 1.60 (m, 4H), 1.77 – 1.84 (m, 4H), 4.38 (t, *J* = 7.8 Hz, 4H),

6.19 (s, 1H), 1.07 (t, *J* = 7.5 Hz, 2H), 7.42 (d, *J* = 8.6 Hz, 2H), 7.67 – 7.72 (m, 4H), 7.86 (d, *J* = 15.2 Hz, 2H), 7.99 – 8.02 (m, 4H). ^{13}C NMR (400 MHz, $CDCl_3$) δ = 13.9, 20.4, 29.6, 42.8, 104.0, 114.4, 120.5, 122.7, 125.1, 125.2, 130.4, 132.9, 139.6, 143.0, 144.4, 160.5, 180.8 ppm. ESI-QTOF (positive ionization) M+H calc. for $C_{33}H_{33}BF_2N_2O_4$: 571.1502; found: 571.1498.

3,3'-((1E,1'E)-(2,2-Difluoro-2H-1λ^3,3,2λ^4-dioxaborinin-4,6-diil)bis(etheno-2,1-diiy))bis(1-butyl-6-methylquinolin-2(1H)-one) **11e**. red solid, yield: 85%. M.p. 234-236 °C. FTIR (ATR): ν = 2953 (=C-H), [1647, 1630] (C=O), 1520 (C=C) cm^{-1}. ^{1}H NMR (400 MHz, $CDCl_3$) δ = 1.06 (t, *J* = 7.3 Hz, 6H), 1.52 – 1.60 (m, 4H), 1.75 – 1.83 (m, 4H), 2.48 (s, 6H), 4.36 (t, *J* = 7.8 Hz, 4H), 6.18 (s, 1H), 7.32 (d, *J* = 8.5 Hz, 2H), 7.49 – 7.51 (m, 4H), 7.87 (d, *J* = 15.3 Hz, 2H), 7.95 (s, 2H), 8.00 (d, *J* = 15.3 Hz, 2H). ^{13}C NMR δ = 14.1, 17.7, 19.7, 31.0, 66.2, 102.5, 119.8, 124.1, 124.8, 125.8, 127.0, 130.8, 135.2, 135.5, 138.7, 145.6, 159.0, 183.6 ppm. ESI-QTOF (positive ionization) M+H calc $C_{35}H_{37}BF_2N_2O_4$: 599.2893; found: 599.2884.

3,3'-((1E,1'E)-(2,2-Difluoro-2H-1λ^3,3,2λ^4-dioxaborinin-4,6-diyl)bis(etheno-2,1-diyl))bis(1-butyl-6-chloroquinolin-2(1H)-one) **11f**. red solid, yield: 91%. M.p. 256-258 °C. FTIR (ATR): ν = 2961 (=C-H), 1645 (2 x C=O), 1520 (C=C) cm^{-1}. ^{1}H NMR (400 MHz, $CDCl_3$) δ = 1.07 (t, *J* = 7.3 Hz, 6H), 1.52 – 1.59 (m, 4H), 1.76 – 1.80 (m, 4H), 4.33 – 4.37 (m, 4H), 6.22 (s, 1H), 7.36 (d, *J* = 9.1 Hz, 2H), 7.62 (dd, *J* = 9.1, 2.4 Hz, 2H), 7.69 (d, *J* = 2.4 Hz, 2H), 7.88 (d, *J* = 15.3 Hz, 2H), 7.94 (s, 2H), 8.00 (d, *J* = 15.3 Hz, 2H). Compound **11f** is barely soluble in $CDCl_3$ and dimethyl sulfoxide, thus, made the registration of a high resolution ^{13}C NMR spectrum impossible. ESI-QTOF (positive ionization) M+H calc. for $C_{33}H_{31}BCl_2F_2N_2O_4$: 639.1800; found: 639.1806.

2.3. General procedure for the synthesis of the *bis*-quinoline decomplexed derivatives 12a-f. A solution of *bis*-quinolin curcuminoid BF_2-complexes **11b-f** (200 mg) in MeOH/DMSO (1:1, 5 mL) was heated under reflux for 1 h. After completion (checked by TLC), the solids formed were collected by filtration, washed cold methanol (2 x 3 mL) and dried in air. No further purification was required.

(1E,4Z,6E)-1,7-bis(2-Butoxy-6-methylquinolin-3-yl)-5-hydroxyhepta-1,4,6-trien-3-one **12a**. Yellow solid, yield: 80%. M.p. 165-168 °C. FTIR (ATR): ν = 2959 (=C-H), 1614 (C=O), 1562 (C=C) cm^{-1}. ^{1}H NMR (400 MHz, $CDCl_3$) δ = 1.09 (t, *J* = 7.4 Hz, 6H), 1.58 – 1.67 (m, 4H), 1.91 – 1.98 (m, 4H), 2.52 (s, 6H), 4.61 (t, *J* = 6.6 Hz, 4H), 5.90 (s, 1H), 7.03 (d, *J* = 15.9 Hz, 2H), 7.48 – 7.52 (m, 4H), 7.77 (d, *J* = 8.4 Hz, 2H), 7.91 (d, *J* = 15.9 Hz, 2H), 8.12 (s, 2H), OH was not observed. ^{13}C NMR (400 MHz, $CDCl_3$) δ = 14.0, 19.6, 21.3, 31.1, 66.6, 102.6, 120.2, 124.9, 126.6, 127.0, 127.1, 132.8, 134.2, 135.5, 138.1, 144.9, 159.6, 183.8 ppm. EI MS (70 eV): *m/z* (%): 550 (M^+, 30), 212 (88), 184 (100).

(1E,4Z,6E)-1,7-bis(2-Butoxyquinolin-3-yl)-5-hydroxyhepta-1,4,6-trien-3-one **12b**. Yellow solid, yield: 70%. M.p. 120-123 °C. FTIR (ATR): ν = 2957 (=C-H), 1628 (C=O), 1560 (C=C) cm^{-1}. ^{1}H NMR (400 MHz, $CDCl_3$) δ = 1.10 (t, *J* = 7.4 Hz, 6H), 1.58 – 1.68 (m, 4H), 1.92 – 1.99 (m, 4H), 4.63 (t, *J* = 6.6 Hz, 4H), 5.91 (s, 1H), 7.04 (d, *J* = 15.9 Hz, 2H), 7.41 (t, *J* = 7.4 Hz, 2H), 7.66 (t, *J* = 7.4 Hz, 2H), 7.76 (d, *J* = 7.9 Hz, 2H), 7.86 (d, *J* = 8.3 Hz, 2H), 7.93 (d, *J* = 15.9 Hz, 2H), 8.21 (s, 2H), OH was not observed. ^{13}C NMR (400 MHz, $CDCl_3$) δ = 14.0, 19.6, 31.1, 66.6, 102.6, 120.4, 124.6, 125.0, 126.9, 127.2, 128.0, 130.6, 135.3, 138.5, 146.6, 160.0, 183.5 ppm. EI MS (70 eV): *m/z* (%): 341 (4), 81 (48), 69 (100).

(1E,4Z,6E)-1,7-bis(2-Butoxy-6-chloroquinolin-3-yl)-5-hydroxyhepta-1,4,6-trien-3-one **12c**. Yellow solid, yield: 75%.

M.p. 205-208 °C. FTIR (ATR): ν = 2963 (=C-H), 1628 (C=O), 1564 (C=C) cm^{-1}. ^1H NMR (400 MHz, $CDCl_3$) δ = 1.10 (t, *J* = 7.3 Hz, 6H), 1.58 – 1.67 (m, 4H), 1.92 – 1.99 (m, 4H), 4.65 (t, *J* = 5.9 Hz, 4H), 5.92 (s, 1H), 7.02 (d, *J* = 15.9, 2H), 7.58 – 7.60 (m, 2H), 7.74 (s, 2H), 7.83 (d, *J* = 8.4 Hz, 2H), 7.91 (d, *J* = 15.9 Hz, 2H), 8.11 (s, 2H), OH was not observed. Compound **12c** is barely soluble in $CDCl_3$ and dimethyl sulfoxide, thus, made the registration of a high resolution ^{13}C NMR spectrum impossible. EI MS (70 eV): *m/z* (%): 425 (12), 367 (22), 69 (100).

3,3'-((1E,3Z,6E)-3-Hidroxy-5-oxohepta-1,3,6-trien-1,7-diyl)bis(1-butylquinolin-2(1H)-one) **12d**. Orange solid, yield: 68%. M.p. 218-220 °C. FTIR (ATR): ν = 2959 (=C-H), [1649, 1605] (C=O), 1555 (C=C) cm^{-1}. ^1H NMR (400 MHz, $CDCl_3$) δ = 1.06 (t, *J* = 7.3 Hz, 6H), 1.52 – 1.61 (m, 4H), 1.75 – 1.83 (m, 4H), 4.63 (t, *J* = 7.8 Hz, 4H), 5.96 (s, 1H), 7.26 – 7.31 (m, 2H), 7.39 (d, *J* = 8.6 Hz, 2H), 7.50 (d, *J* = 15.7 Hz, 2H), 7.60 – 7.66 (m, 4H), 7.73 (d, *J* = 15.7 Hz, 2H), 7.92 (s, 2H), OH was not observed. ^{13}C NMR (400 MHz, $CDCl_3$) δ = 13.9, 20.4, 29.6, 42.7, 103.4, 114.2, 120.6, 122.4, 126.3, 128.2, 129.8, 131.6, 136.1, 139.1, 140.2, 160.7, 183.8 ppm. EI MS (70 eV): *m/z* (%): 522 (M^+, 3), 129 (23), 43 (100).

3,3'-((1E,3Z,6E)-3-Hydroxy-5-oxohepta-1,3,6-trien-1,7-diyl)bis(1-butyl-6-methylquinolin-2(1H)-one) **12e**. Orange solid, yield: 75%. M.p. 224-226 °C. FTIR (ATR): ν = 2951 (=C-H), [1647, 1600] (C=O), 1560 (C=C) cm^{-1}. ^1H NMR (400 MHz, $CDCl_3$) δ = 1.06 (t, *J* = 7.3 Hz, 6H), 1.51 – 1.60 (m, 4H), 1.75 – 1.83 (m, 4H), 2.46 (s, 6H), 4.35 (t, *J* = 7.7 Hz, 4H), 5.97 (s, 1H), 7.28 (d, *J* = 9.7 Hz, 2H), 1.41 – 7.43 (m, 4H), 7.47 (d, *J* = 15.9 Hz, 2H), 7.73 (d, *J* = 15.7 Hz, 2H), 7.85 (s, 2H),), OH was not observed. ^{13}C NMR (400 MHz, $CDCl_3$) δ = 13.7, 20.4, 29.6, 42.6, 63.6, 102.9, 114.1, 120.7, 126.4, 128.1, 129.3, 131.8, 132.9, 136.1, 137.3, 139.6, 160.6, 183.8 ppm. EI MS (70 eV): *m/z* (%): 341 (8), 81 (48), 69 (100).

3,3'-((1E,3Z,6E)-3-Hydroxy-5-oxohepta-1,3,6-trien-1,7-diyl)bis(1-butyl-6-chloroquinolin-2(1H)-one) **12f**. Yellow solid, yield: 80%. M.p. 268-270 °C. FTIR (ATR): ν = 2961 (=C-H), [1653, 1612], (C=O), 1548 (C=C) cm^{-1}. ^1H NMR (400 MHz, $CDCl_3$) δ = 1.09 (t, *J* = 7.4 Hz, 6H), 1.59 – 1.64 (m, 4H), 1.90 – 1.97 (m, 4H), 4.60 (t, *J* = 6.6 Hz, 4H), 5.88 (s, 1H), 7.01 (d, *J* = 15.9 Hz, 2H), 7.35 (dd, *J* = 8.4, 1.6 Hz, 2H), 7.66 (d, *J* = 8.6 Hz, 2H), 7.84 (d, *J* = 1.8 Hz, 2H), 7.87 (d, *J* = 15.9 Hz, 2H), 8.13 (s, 2H), OH was not observed. ^{13}C NMR (101 MHz, $CDCl_3$) δ = 14.0, 19.5, 31.0, 66.8, 102.8, 120.5, 123.3, 125.4, 126.3, 127.5, 129.0, 135.0, 136.5, 137.9, 147.2, 160.6, 183.3 ppm. EI MS (70 eV): *m/z* (%): 590/592 (M^+, 46/35), 260 (45).

3. Results and discussion

3.1. Synthesis of new bis-quinolin curcuminoid BF_2-complexes and their decomplexed derivatives

Scheme 1 presents the synthetic route for the preparation of the new *bis*-quinolin based difluoroboron-curcuminoid complexes **11b-f**. Initially, we obtained the donor units 3-formyl-2-alkoxy-quinolines (*O*-butylated) **10a-c** and 3-formyl-2-oxo-quinolines (*N*-butylated) **10d-f** via Meth-Cohn reactions, mediated by acid hydrolysis of chloro-derivatives **8** and *O*-, *C*-alkylation of intermediates **9** [18]. Subsequently, the synthesis of the new BF_2-complexes **11b-f** was performed following the methodology reported by Liu et al. [22]. In this approach, the acetylacetone boronite (AA-BF_2) was generated *in situ*, by treating acetylacetone with $BF_3.Et_2O$ at 80°C for 2h. After cooling, the condensation reaction was carried out by adding a mixture of the formylquinolines **10a-f**, *n*-butylamine (n-$BuNH_2$) and tributyl borate $B(OBu)_3$ in toluene, to the AA-BF_2 solution. The thin-layer chromatography (TLC) analysis showed the formation of a single

product. The solids formed were filtered under reduced pressure and washed repeatedly with toluene, affording pigments **11b-f** in 75-94% yield. All BF_2-complexes **11** were characterized by ^1H and ^{13}C NMR and mass spectrometry. The ^1H NMR spectrum of the BF_2-complex **11b**, run in $CDCl_3$, showed a singlet at 6.14 ppm, corresponding to the proton H-4´, and two doublets at 7.25 and 8.22 ppm (J = 15.6 Hz), assigned to protons 1´ and 2´ of the *α,β*-unsaturated moiety. Therefore, confirming a satisfactory condensation reaction between AA-BF_2 and **10**, as well as, *E* configuration of the new double bonds formed. In the ^{13}C NMR spectrum, the total expected signals (i.e. 13) for BF_2-complex **11b** were observed (see supplementary Information). The mass spectrum confirmed the formation of the desired BF_2-complex **11b** and allowed to observe the peak of the molecular ion with *m/z* 598. The ^1H, ^{13}C NMR spectra for the remaining BF_2-complexes **11b-f** were similar, confirming the generality of the process (supplementary Information).

Scheme 1. Synthesis of *bis*-quinolin curcuminoid BF_2-complexes **11b-f.**

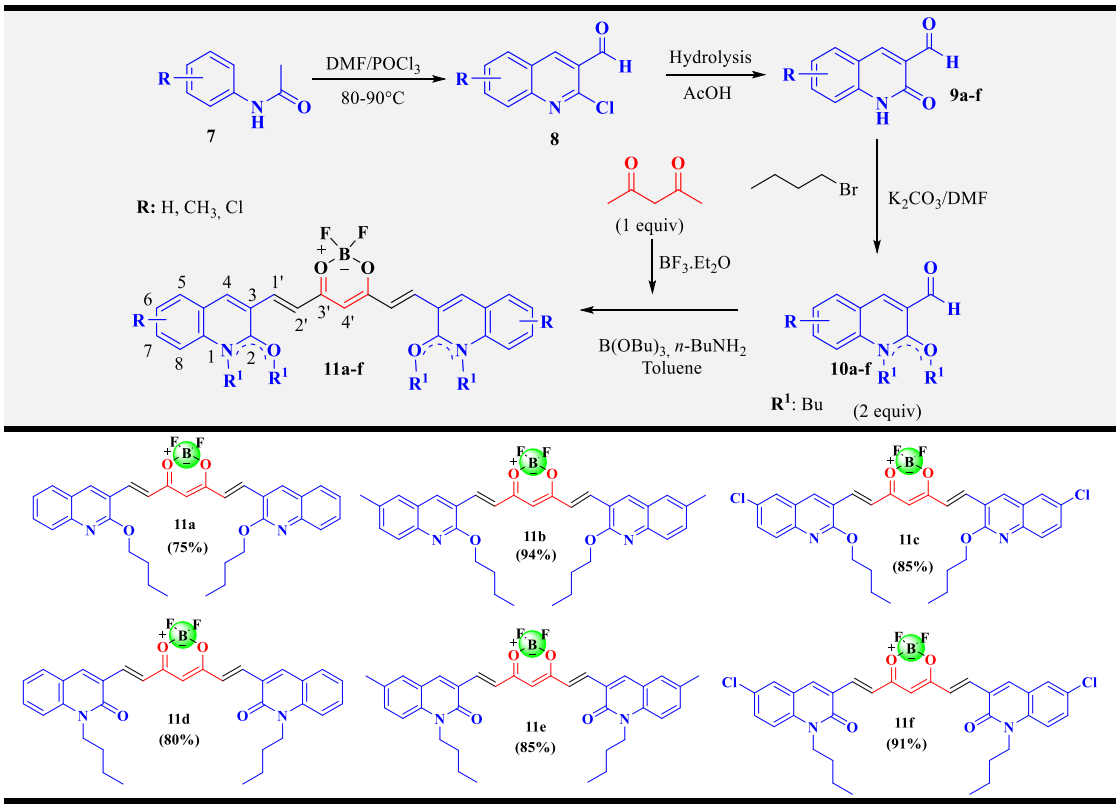

Once the BF_2-complexes **11** were obtained, subsequently, we performed the decomplexation in order to obtain their corresponding *bis*-quinolin curcuminoid derivatives **12a-f.** Thus, the treatment of BF_2-complexes **11** with a mixture MeOH/DMSO (1:1 ratio) under reflux for 1h [22], afforded the decomplexed derivatives **12a-f** as yellow solids in 68-85%, as shown in Scheme 2. The ^1H and ^{13}C NMR spectra showed that decomplexed derivatives **12a-f** exist in their enolic tautomers, as usual [23], instead of their diketonic ones. In consequence, in the ^1H NMR spectrum of the decomplexed derivative **12a** a singlet was observed at 5.90 ppm assigned to the proton H-4', confirming the formation of the enolic tautomer, and two doublets at 7.03 and 7.91 ppm (J = 15.9 Hz), corresponding to the protons 1´ and 2´ of the α,β-unsaturated moiety, confirming the *E* configuration of the new double bonds formed in the decomplexed derivatives **12**. In the ^{13}C NMR spectrum, the total expected signals (18) were observed for the decomplexed derivative **12a** (including the absence of aliphatic carbon CH_2 due to the preferred enol tautomeric form). Finally, the

mass spectrum of **12a** corroborated the decomplexation process, observing the peak of the expected molecular ion with *m/z* 550.

Scheme 2. Synthesis of the *bis*-quinoline decomplexed derivatives **12a-f.**

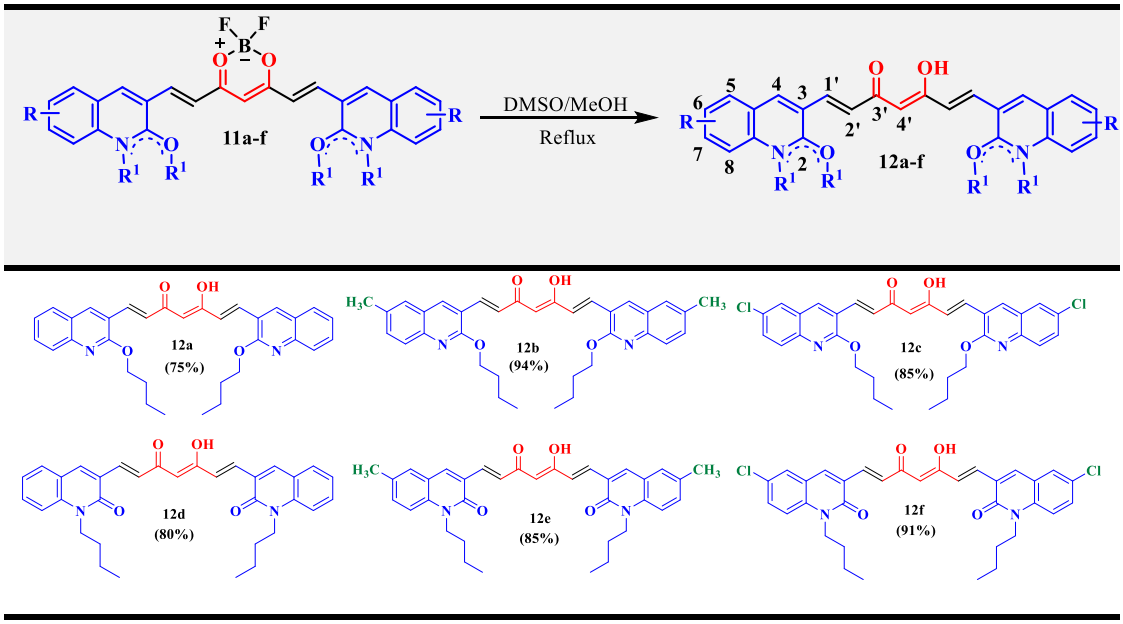

3.2. Absorption and emission properties

Figure 3 and Table 1 show the results of the absorption and emission measures of the BF_2-complexes **11b-f,** as well as, their corresponding decomplexed derivatives **12a-f**, performed at a concentration of $1x10^{-5}$ M, using dichloromethane as solvent. The absorption spectra showed intense bands between 413-512 nm, likely due to CT-type transitions and weak bands around 300 nm, which are attributed to n-π* transitions (Figure 3a,b). In turn, we observed in all studied compounds a high absorption intensity, as reflected in their values of ε (molar absorptivity), ranging between $3.41x10^4$ - $9.99x10^4$ (see Table 1). The emission spectra (Figure 3c,d) were measured at 355 nm as the excitation wavelength of prodan provided the fluorescence standard.

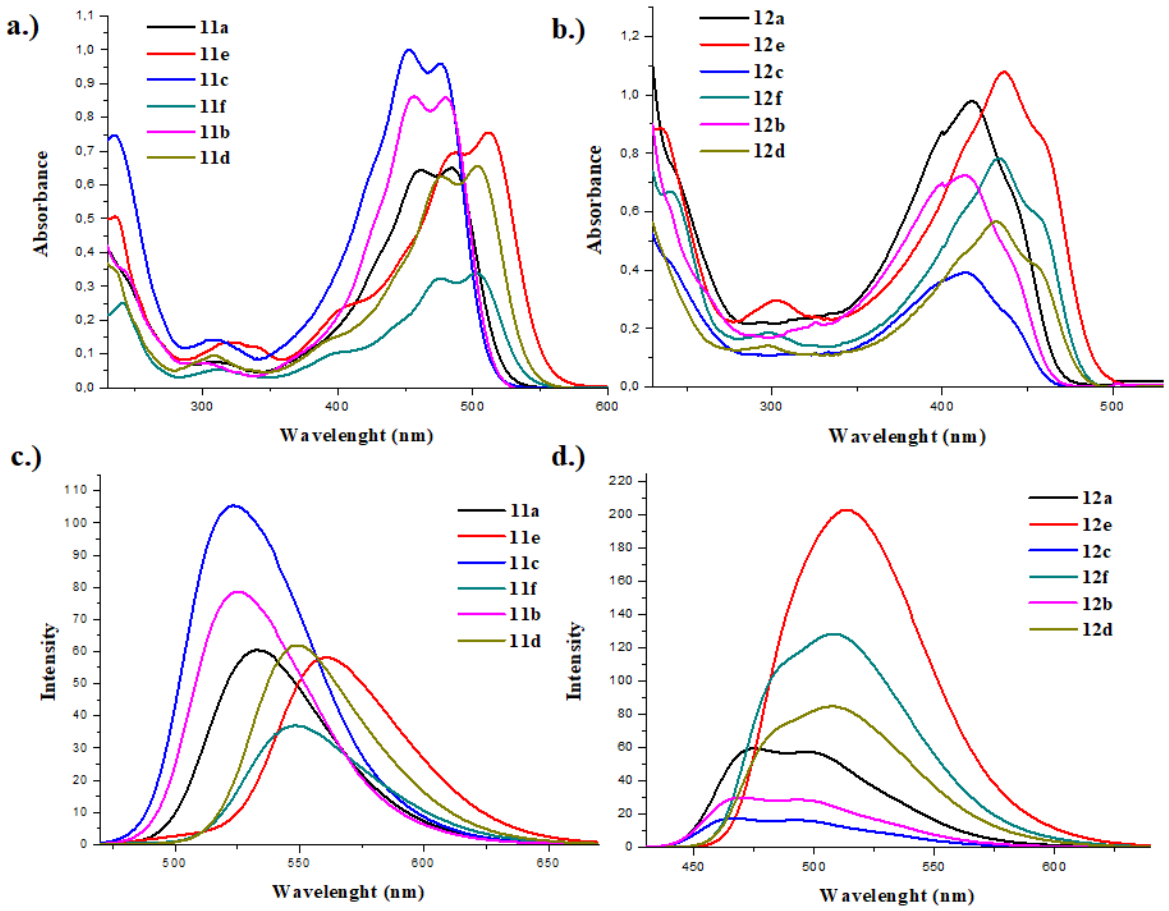

Figure 3. CH_2Cl_2 absorption spectra of: **(a)** BF_2-complexes **11b-f**; **(b)** decomplexed derivatives **12a-f** and emission spectra of: **(c)** BF_2-complexes **11b-f**; **(d)** unpacked decomplexed derivatives **12a-f**.

Table 1. Measured values of absorption and emission spectra in CH_2Cl_2 as the solvent, for BF_2-complexes **11b-f** and decomplexed derivatives **12a-f**; at an approximate concentration of $1x10^{-5}$ M

Compound	λ^1_{abs}(nm)/ε($M^{-1}cm^{-1}$) $x10^{-4}$	λ^2_{abs}(nm)/ε($M^{-1}cm^{-1}$) $x10^{-4}$	λ^1_{ems}(nm)[a]	λ^2_{ems}(nm)[a]	Δλ(cm^{-1})	ϕ_F[b]
11b	461/6.44	485/6.50	533	-	208333	$8.85x10^{-4}$
11b	458/8.62	480/8.59	525	-	222222	$1.17x10^{-3}$
11c	451/9.99	476/9.59	524	-	208333	$1.89\ x10^{-3}$
11d	478/6.52	503/6.56	549	-	217391	$9.48x10^{-4}$
11e	486/7.50	512/6.95	560	-	208333	$8.07x10^{-4}$
11f	476/3.41	503/3.39	548	-	222222	$6.98x10^{-4}$
12a	418/9.82	-	475	499	175438	$7.83x10^{-4}$
12b	458/8.72	-	469	494	909090	$2.30x10^{-4}$
12c	413/3.95	-	466	493	188679	$1.74x10^{-4}$
12d	432/5.71	-	483	507	196078	$2.68x10^{-3}$

12e	435/10.7	-	-	513	128205	$7.58x10^{-3}$
12f	434/7.89	-	486	508	192307	$4.38x10^{-3}$
Prodan	355/1.79	-	439	-	-	0.98

[a]Measurements in λ_{exc} of PRODAN (355 nm), used as a fluorescence standard.[b] Values relative to the quantum fluorescence performance of the standard, $\phi_s = 0.98$.

The BF_2-complexes **11d-f** showed a better chromophore system compared to BF_2-complexes **11b-c**, as suggested by the analysis of absorption spectra of the synthesized BF_2-complexes **11b-f** (Figure 3a) and the fluorescence emission spectra (Figure 3c), which revealed that the corresponding wavelengths for the BF_2-complexes of *N*-butylquinolones are displaced towards the red compared to the BF_2-complexes of *O*-butylquinolines. We also observed that for BF_2-complexes **11b** and **11e**, which contain an electrodonor group such as $-CH_3$ in the heterocyclic ring, the absorption, and emission bands undergo a slight bathochromic displacement in comparison with the unsubstituted BF_2-complexes **11b** and **11d**, whereas the displacement is hypsochromic in the presence of an electron-withdrawing group such as -Cl (see Table 1). On the other hand, we observed non-regular tendency in the absorption (Figure 3b) and emission (Figure 3d) spectra of decomplexed derivatives **12a-f** (see Table 1), suggesting the presence of a non-rigid conjugate system and a weaker acceptor behavior than the BF_2-complexes. This behavior is consistent with the photophysical characteristics of several BF_2-complex and their curcumin analogues reported in the literature [24].

The emission spectra of BF_2-complexes **11b-f** evidenced an intramolecular charge transfer (ICT) process from the quinolinic ring (donor fragment) toward the moiety that contains the BF_2 functionality (acceptor fragment). This process is observed via deactivation of the fluorescence intensity when passing from an electron-withdrawing substituent, such as –Cl (ϕ_f: 1.89 $x10^{-3}$), to an electron-donor substituent, such as $-CH_3$ (ϕ_f: 8.85 $x10^{-4}$). Therefore, a donor substituent favors deactivation by an ICT process, whereas an acceptor substituent favors deactivation to a lesser extent by the ICT process and mostly by fluorescence. Also, the *N*-butylated BF_2-complexes **11d-f** presented lower fluorescence intensity (see ϕ_f in Table 1), than their corresponding *O*-butylated ones **11b-c**, indicating that the *N*-butyl substituent behave as a better electron-donor than the *O*-butyl substituent. It is important to note that derivatives **11b-c** (quinolines), have a higher aromatic character compared to derivatives **11d-f** (quinolones). In other words, the heterocyclic fragments greatly affect the spectroscopic behavior of the resultant curcumin-BF_2 complexes. Table 1 also shows the smaller values of Stoke´s displacements in BF_2-complexes **11** ($\Delta\lambda$: 222222-208333 cm^{-1}) when comparing with decomplexed derivatives **12** ($\Delta\lambda$: 909090-128205 cm^{-1}). This finding is associated with a greater flexibility in decomplexed derivatives **12**, which consume the energy absorbed in motion and other non-radiative processes, whereas more rigid BF_2-complexes **11** lose less energy due to non-radiative processes only.

Additionally, the emission spectra of BF_2-complexes **11b-f** showed a single emission band, in contrast to the decomplexed derivatives **12a-f** with their two deactivation pathways (Figure 3d). These results are likely an outcome of the decomplexed derivatives **12a-f** that can be deactivated from two close excitonic states of energy found in a keto-enolic equilibrium, as shown in Figure 4. Interestingly, this behavior does not correspond to Kasha's rule [25]. Therefore, a titration was performed with trifluoroacetic acid (TFA) (Figure 5) to disfavor the keto-enolic equilibrium shown in Figure 4. To achieve that, we selected compounds **12b** and **12d** that have two emission bands, (see Figure 3d). In Figure 5, we decreased the fluorescence intensity of those two compounds by increasing the number of TFA equivalents. In turn, compound **12d** showed a single band without a shoulder (Figure 5b) and a marked deactivation of the emission of the protonated species, an expected behavior when the keto-enolic equilibrium is disrupted. The latter behavior can be clearly attributed to excited state intramolecular proton transfer (ESIPT), which was described by Joo et al. [26] for similar systems, but also could be associated to two close vibronic structures.

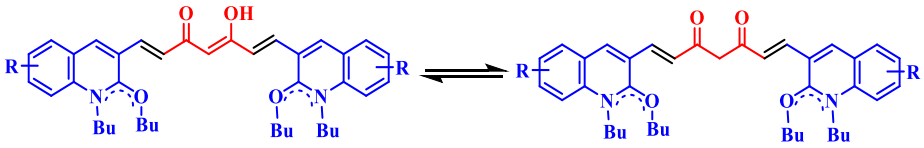

Figure 4. Keto-enolic equilibrium for decomplexed derivatives **12a-f**

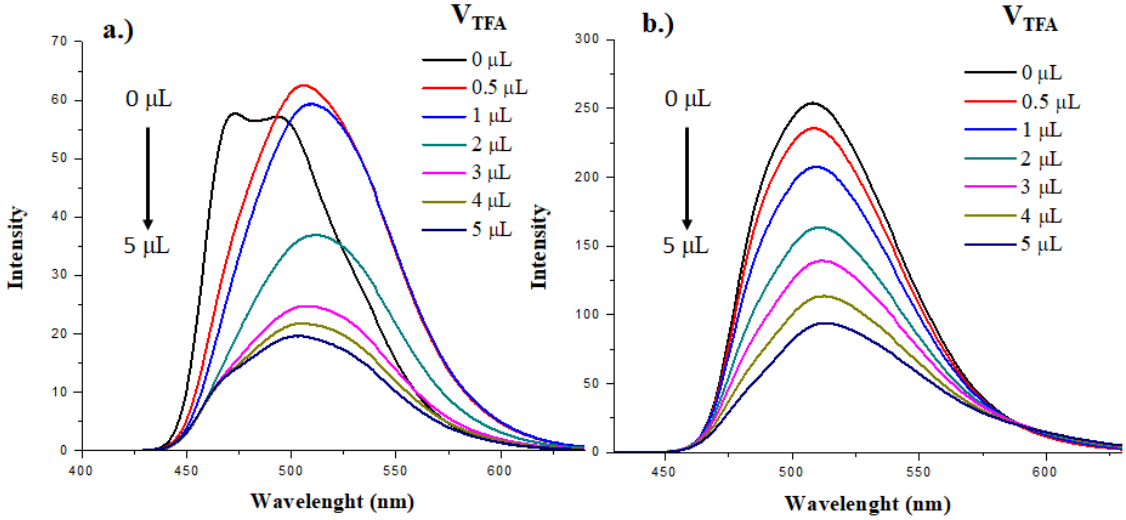

Figure 5. Fluorescence spectra of decomplexed derivatives (a) **12b**; (b) **12d** at a concentration of $5x10^{-5}$ M, titrated with TFA

Fluorescence Quantum yield (Φ_F) were calculated in Equation 1, using Prodan as standard in dichloromethane (DCM) ($\Phi_F^{std} = 0.98$) [27].

$$\phi_F = \phi_F^{std} \frac{FA^{std}In^2}{F^{std}AI^{std}n_{std}^2} \qquad \text{Eq. (1)}$$

Where F and F^{std} are the areas under the fluorescence curves of products **11b-f**, **12a-f,** and the standard, respectively. A and A^{std} correspond to the absorbance of the sample and the standard, I and I^{std} are the relative intensities of the excitation light and n^2 and n^2_{std} are the refractive indices of the solvents used for the sample and the DCM standard. This estimation showed that the fluorescence quantum yield (Φ_F) reached relatively good values (see Table 1).

Subsequently, a solvatochromic study was performed for BF_2-complexes **11b**, **11e** and **11c** and derivatives **12b** and **12e**, using a binary mixture of CH_2Cl_2/MeOH as solvent. The selection of these compounds occurred because: (i) their structural characteristics and (ii) the possibility to compare their structure under a change in polarity of the solvent mixture. For BF_2-complex **11b** (*O*-butyl, R = -CH_3), we noticed that when the percentage of MeOH increases the fluorescence intensity decrease (see Φ_F in Table 2). Consequently, there is an intramolecular charge transfer, since **11b** derivative are strongly dependent on solvent polarity; the emission intensity of the **11b** decreases progressively with increasing solvent polarity, which is consistent with the stabilization of the charge separation state in the emissive state when polar solvents are used. On the other hand, Figure 6b shows that λ_{ems} for this BF_2-complex did not vary significantly when the polarity of the solvent varies. The same analysis applied to the decomplexed derivative **12b** (*O*-butyl, R = -CH_3) revealed that the fluorescence intensity behaves randomly (Figure 7a), this suggests that the charge separation state in the emissive state did not depend on the solvent polarity effect, possibly due to the non-rigid *bis*-quinoline-curcumine bonds compared to the rigid BF_2-complex **11b**. In the normalized fluorescence spectrum for this compound (Figure 7b), a slight bathochromic shift is distinguished by increasing the polarity of the solvent system from 95/5% CH_2Cl_2/MeOH (475 nm) to 75/25% CH_2Cl_2/MeOH (503 nm) (see Table 2), thus suggesting the presence of a weak intramolecular charge transfer process or an excited state intramolecular proton transfer (ESIPT).

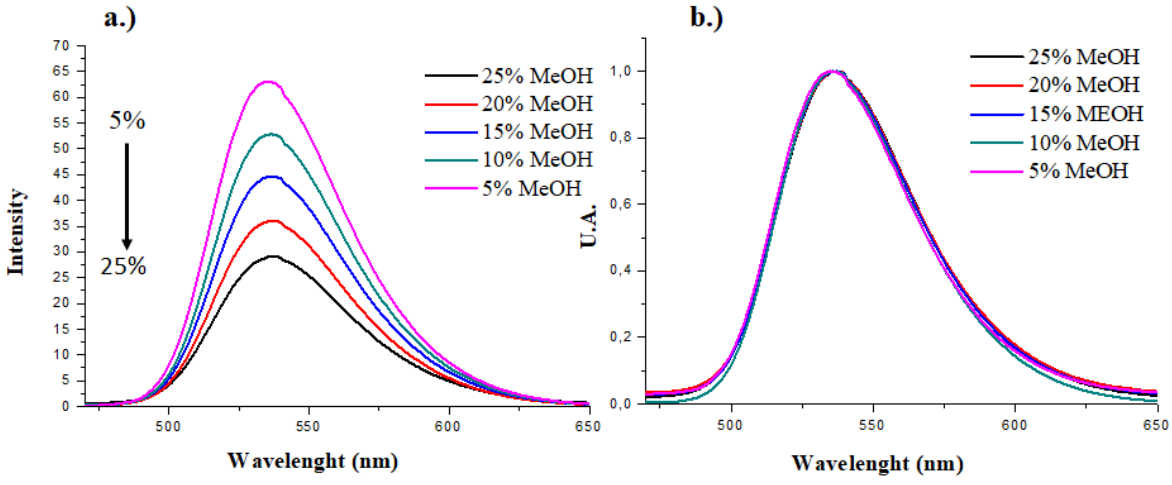

Figure 6. Fluorescence emission spectrum of BF_2-complex **11b** at different ratios of the CH_2Cl_2/MeOH solvent system **(a)** without normalization and **(b)** normalized

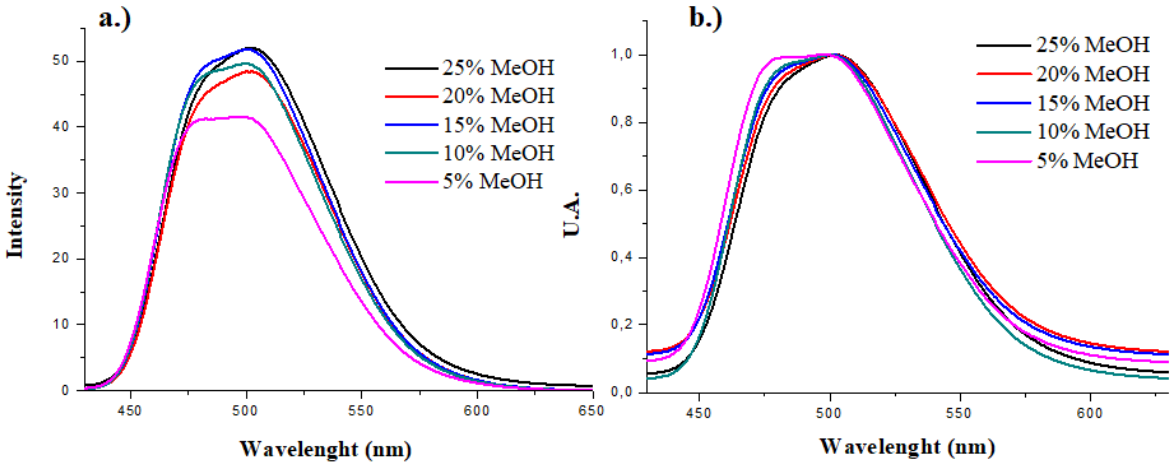

Figure 7. Fluorescence emission spectrum of the decomplexed derivative **12b**, at different ratios of the CH_2Cl_2/MeOH solvent system **(a)** without normalization and **(b)** normalized

Table 2. Measured absorption and emission values in CH_2Cl_2/MeOH as solvent, for compounds **11b**, **11c**, **11e**, **12a** and **12e** at an approximate concentration of $1x10^{-5}$ M

% MeOH	BF_2-complex 11b		BF_2-complex 11e		BF_2-complex 11c		Dec. deriv. 12b		Dec. deriv. 12e	
	λ^1_{ems} (nm)[a]	Φ_F[b]	λ^1_{ems} (nm)[a]	Φ_F[b]	λ^1_{ems} (nm)[a]	Φ_F[b]	λ^1_{ems} /λ^2_{ems} (nm)[a]	Φ_F[b]	λ^1_{ems} (nm)[a]	Φ_F[b]
5	535	$8.87x10^{-4}$	562	$3.57x10^{-4}$	525	$1.87x10^{-3}$	489	$7.38x10^{-4}$	521	$3.65x10^{-3}$
10	536	$8.8x10^{-4}$	565	$3.25x10^{-4}$	525	$1.20x10^{-3}$	501	$1.11x10^{-3}$	523	$5.10x10^{-3}$
15	537	$4.34x10^{-4}$	564	$1.95x10^{-4}$	527	$1.44x10^{-3}$	501	$1.19x10^{-3}$	526	$4.49x10^{-3}$
20	537	$2.78x10^{-4}$	565	$1.66x10^{-4}$	527	$1.24x10^{-3}$	502	$1.02x10^{-3}$	528	$4.18x10^{-3}$
25	538	$1.93x10^{-4}$	565	$7.80x10^{-5}$	528	$1.17x10^{-3}$	503	$1.19x10^{-3}$	528	$5.13x10^{-3}$

Measured in λ_{exc} of PRODAN (355 nm), used as a fluorescence standard. [b.] Values relative to the quantum fluorescence performance of the standard, $\phi_s = 0.98$.

Likewise, the solvatochromic study performed for the BF_2-complex **11e** (*N*-butyl, R = $-CH_3$) showed a marked deactivation of the fluorescence band (Figure 8a) (see Φ_F in Table 2). Based in this observation, the *N*-alkylamine functionality in **11e** behaves as a moiety with better electron-donor characteristic (Figure 9). To confirm the above, solvatochromic experiments were carried out for the decomplexed derivative **12e** (*N*-butyl, R = $-CH_3$). Figure 10a shows that the emission intensity of derivatives **12e** and **12a** did not show a dependent relationship with the polarity of the solvent system, likely an outcome of the weak electron-acceptor capacity of the flexible *bis*-quinoline-curcuminoid moiety. Interestingly, in this case, when the polarity of the solvent system increases, the λ_{em} moves towards red (~ 14 nm)

(see Table 2) (Figure 10b), thus confirming the greater electron-donor force of the *N*-butylamine functionality. To better show the solvatochromic behavior of the measured compounds, a ratio between emission intensity and absorbance was made, where it is evidenced that the behavior of the quantum yield with respect to the variation of the polarity of the solvent is in accordance with the phenomena described before [26] (see table 3). For instance, for compound **11b** the emission intensity/absorbance ratio decreases with respect to system solvent polarity. On the other hand, for compound **12b** the values of intensity/absorbance ratio are randomly distributed in accordance with the system solvent polarity.

Table 3. Values for intensity of emission/absorption ratios in CH_2Cl_2/MeOH as solvent, for compounds **11b**, **11c**, **11e**, **12b** and **12e** at an approximate concentration of $1x10^{-5}$ M.

% MeOH	**BF_2-complex 11b**	**BF_2-complex 11e**	**BF_2-complex 11c**	**Dec. deriv. 12b**	**Dec. deriv. 12e**
	Ratio int em/Abs	Ratio int em/Abs	Ratio int em/Abs	Ratio int em/Abs	Ratio int em/Abs
5	84.65	65.23	146.35	78.52	173.06
10	98.41	70.32	100.75	104.05	224.36
15	58.47	52.60	134.01	104.81	169.97
20	46.64	55.09	104.42	99.17	191.01
25	39.48	29.90	105.17	106.38	228.32

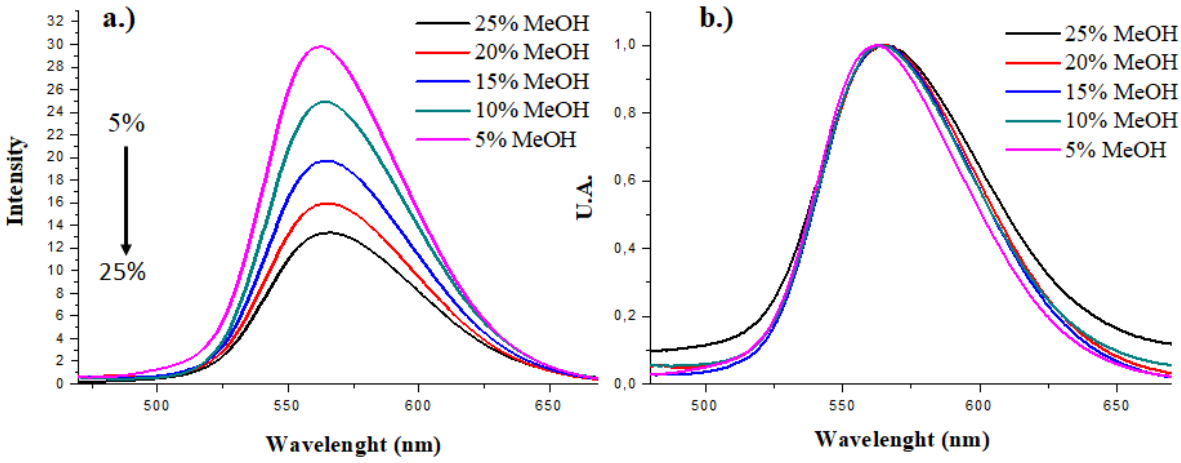

Figure 8. Fluorescence emission spectrum of BF_2-complex **11e**, at different ratios of the CH_2Cl_2/MeOH solvent system **(a)** without normalization and **(b)** normalized

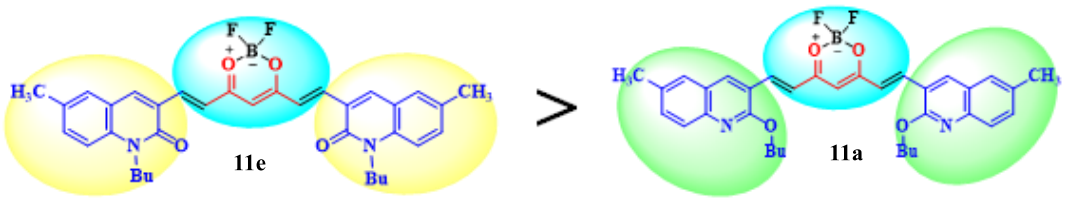

Figure 9. Comparison of the electron-donor capacity between the different quinolinic moieties of BF_2-complexes **11b** and **11e**, according to the photophysical measurements.

Subsequently, solvatochromic studies were performed for BF_2-complex **11c**, which has chlorine atoms in the C-6 position of the quinoline rings. Figure 10c shows that the emission intensity did not depend on the polarity of the solvent system, but the normalization of all the emission bands (Figure 10d) revealed a slight red shift (~ 1 nm) (Table 2). This result indicates the presence of an intramolecular charge transfer but attenuated by the chlorine atom with its characteristic electron-withdrawing effect, which decreased the electron-donor capability of the quinolinic system.

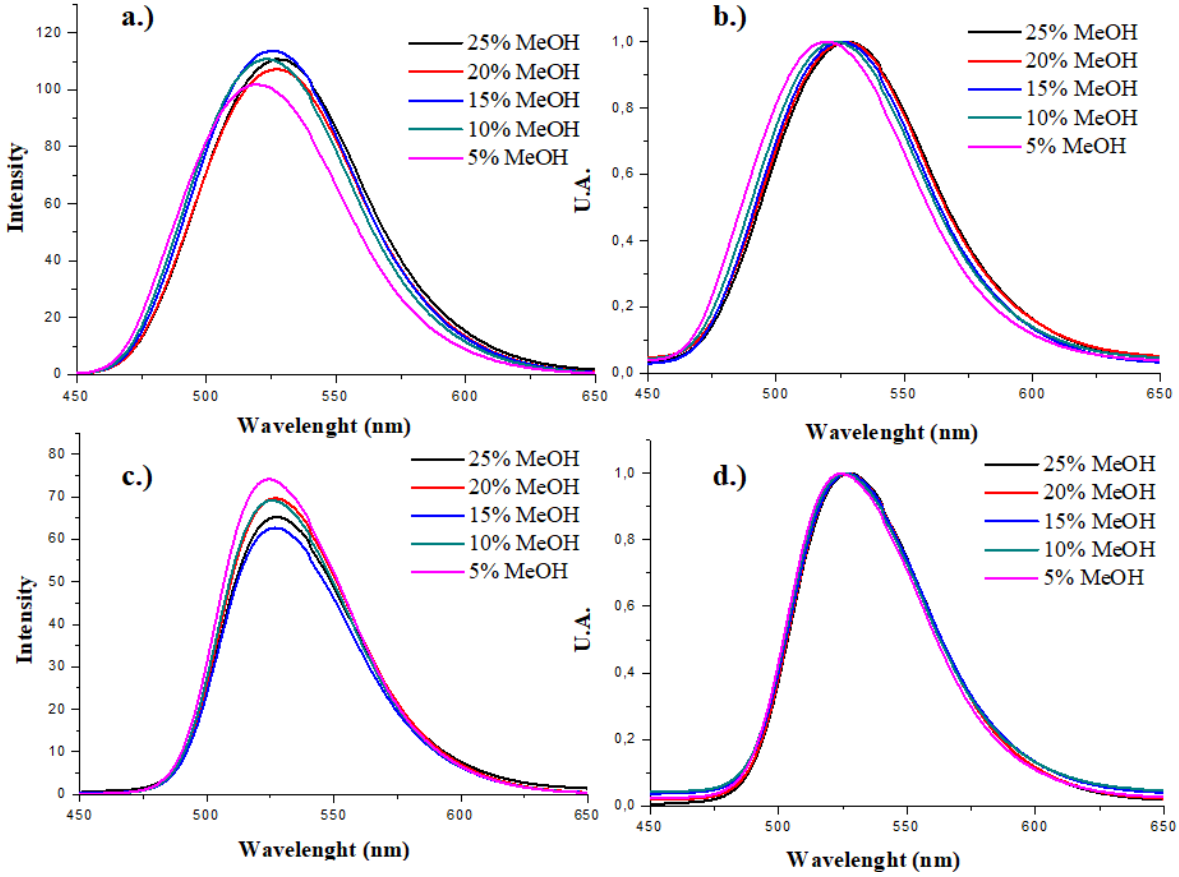

Figure 10. Fluorescence emission spectra of (I): decomplexed derivative **12e**, **(a)** without normalization and **(b)** normalized. (II) BF_2-complex **11c**, **(c)** without normalization and **(d)** normalized, both at different ratios of the CH_2Cl_2/MeOH solvent system

3.3. Theoretical calculations

A computational analysis allowed to determine the characteristics of the most significant electronic transitions; for this

purpose, the structures of compounds **11b**, **11c**, **11e** and **12b** were optimized at DFT level with B3LYP hybrid functional and 6-31G++ basis set, in vacuum. Optimized structures helped to establish the different electronic properties associated with the structure. For example, to study the differences (i) between **11b** and **11e** induced, respectively, by the *O*-substitution and the *N*-substitution and (ii) between **11b** and **12b** with the influence of $–BF_2$ functionality on the π-conjugate system. Finally, the optimized structures contributed to deduce the effect of the methyl substituent (electron-donor) in **11b** in comparison to the chlorine substituent (electron-withdrawing) in **11c**. Additionally, we simulated the electronic transitions of the absorption spectra and a continuous polarization model (PCM) with dichloromethane as solvent and estimated the characteristics of absorption modes (Table 4).

Table 4. Calculated characteristics of linear absorption transitions for compounds **11b, 12a, 11e,** and **11c.**

Compound	Excited Status	Composition	Energy (eV)	λ_{abs} (nm)	Oscillator Force
11b	S_1	HOMO → LUMO (0.67786)	2.482	499.6	1.8711
	S_2	HOMO-1 → LUMO (0.67526) HOMO → LUMO (0.18874)	2.568	482.8	0.0356
12a	S_1	HOMO-1 → LUMO (0.19887) HOMO → LUMO (0.66753)	3.111	398.6	0.9288
11e	S_1	HOMO → LUMO (0.65354)	2.245	552.4	0.7852
	S_2	HOMO-1 → LUMO (0.65261) HOMO → LUMO (0.25646)	2.414	513.6	0.0643
11c	S_1	HOMO → LUMO (0.69744)	2.525	491.0	1.8821
	S_2	HOMO-1 → LUMO (0.69493) HOMO → LUMO (0.16984)	2.728	454.4	0.1574

The calculated values of λ_{abs} are very close to the experimental values of λ^2_{abs} for the compounds **11b**, **11c,** and **11e**, and for the λ^1_{abs} value in **12b** (Table 2). These results combined with the transitions of border molecular orbitals as described in Table 4, demonstrated that the transitions of maximum absorption for **11b**, **11c,** and **11e** should be observed as two wide bands resulting from the sum of S_1 (HOMO→LUMO) with S_2 (HOMO-1→LUMO; HOMO→LUMO). On the other hand, the behavior for maximum absorption transitions for compound **12b** must be presented as broadband with the presence of one or more shoulders product of S_1, which is composed of the combination of two transitions (HOMO-1→LUMO; HOMO→LUMO) in different ratios. To describe these behaviors, Figure 11 shows the topology of the border orbitals involved in the electronic transitions.

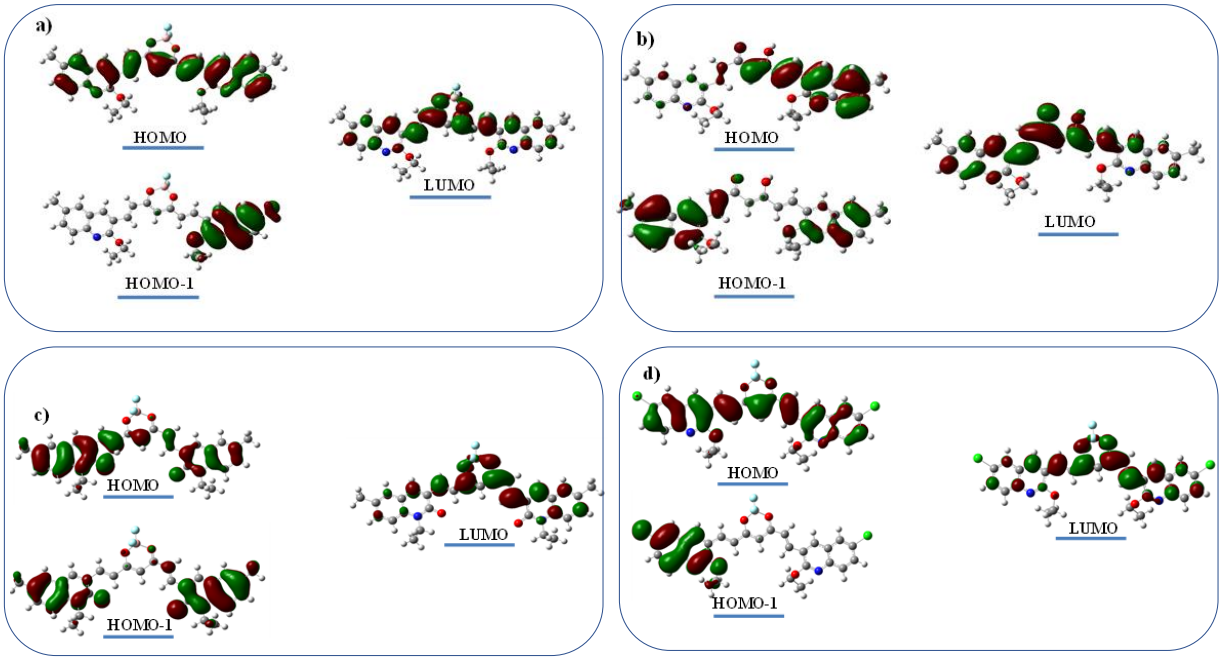

Figure 11. Topology of the border orbitals calculated for **a) 11b**, **b) 12a**, **c) 11e** and **d) 11c** with a Bohr tolerance.

The topological analysis of the boundary orbitals calculated for compound **11b** used as a reference took into account that: the transition HOMO→LUMO and HOMO-1→LUMO have an ICT character from the quinolinic rings to the boron complex suggesting the presence of a D-A type system. Besides, for compound **12b** the two electronic transitions HOMO-1→LUMO and HOMO→LUMO had a strong character $\pi-\pi^*$ given the weaker electron-acceptor force of the α,β–unsaturated system and the free rotation thereof. In the case of compound **11e**, a strong ICT character become evident since the electronic distribution in HOMO and the HOMO-1 is mainly located in the quinoline rings that act as electron-donors. The little participation of the cyclic system of the BF_2-complex in the above occupied molecular orbitals contrasts to LUMO topology, which has an electronic distribution with greater participation of the BF_2 functionality and a small participation on quinoline rings. In summary, *N*-butylated quinolines act more effectively as electron-donors than the *O*-butylated ones, and their molecules have a D-A-D type system. Finally, compound **11c** showed similar HOMO-1, HOMO, and LUMO topology than for compound **11b**, but with an attenuated ICT character of the HOMO-1→LUMO transition due to the electron-withdrawing action of the chlorine atoms attached to the quinolinic rings, as evidenced in the LUMO by the significant electronic participation on the quinolinic rings.

4. Conclusions

In summary, we synthesized new series of *bis*-quinolin curcuminoid BF_2-complexes **11b-f** and and their decomplexed

derivatives **12a-f**, through a convergent synthetic methodology with good reaction yields, providing an alternative source of chromophoric organic systems susceptible to structural characteristics. After measuring their absorption and fluorescence spectra, the *N*-butylated derivatives showed a higher chromophore character and better push-pull characteristics than the *O*-butylated analogues. In addition, we found that the methyl group attached to the quinolinic rings of the **11b**, **11e**, **12a**, and **12e** structures, favored the charge transfer processes, whereas this process is disfavored in compounds that have an electron-withdrawing group such as chlorine attached to the same rings (i.e. **11c**, **11f**, **12c**, and **12f**) when comparing with the unsubstituted derivatives (**11b**, **11d**, **12a**, and **12d**). These results were confirmed via computational calculations at DFT level that optimized the TD-DFT structures, thus allowing the simulation of electronic transitions. For compounds (**11b**, **11e**, **12a**, and **12e**) the HOMO and HOMO-1 are mainly located between the quinolinic rings, while the LUMO is located on the BF_2 functionality of the BF_2-complexes (i.e. **11b**, **11e**), as well as, on the 1,2-dicarbonyl system for the decomplexed derivatives (i.e. **12a**, **12e**).

Conflicts of Interest

None

Acknowledgement. The authors gratefully acknowledge COLCIENCIAS, CIBioFi, Universidad del Valle, and Universidad del Norte for financial support.

References

[1] G.H. Elgemeie, R.A. Mohamed, Microwave synthesis of fluorescent and luminescent dyes (1990-2017), J. Mol. Struct. 1173 (2018) 707–742. doi:10.1016/j.molstruc.2018.06.101.

[2] J.M. Chem, D.G. Patel, N.M. Bastianon, P. Tongwa, J.M. Leger, V. Timofeeva, G.P. Bartholomew, Modification of nonlinear optical dyes for dye sensitized solar cells: a new use for a familiar acceptor, J. Mater. Chem. 21 (2011) 4242–4250. doi:10.1039/c0jm03774e.

[3] M.L. Agazzi, M.B. Ballatore, A.M. Durantini, E.N. Durantini, A.C. Tomé, BODIPYs in antitumoral and antimicrobial photodynamic therapy: An integrating review, J. Photochem. Photobiol. C Photochem. Rev. 40 (2019) 21–48. doi:10.1016/j.jphotochemrev.2019.04.001.

[4] M.T. Hill, M.C. Gather, Advances in small lasers, Nat. Photonic. 8 (2014) 908–918.

doi:10.1038/nphoton.2014.239.

[5] E. Kim, A. Felouat, E. Zaborova, J.-C. Ribierre, J.W. Wu, S. Senatore, C. Matthews, P.-F. Lenne, C. Baffert, A. Karapetyan, M. Giorgi, D. Jacquemin, M. Ponce-Vargas, B. Le Guennic, F. Fages, A. D´Aléo, Borondifluoride complexes of hemicurcuminoids as bio-inspired push-pull dyies for bioimaging, Org. Biomol. Chem. 14 (2016) 1311–1324. doi:10.1039/C5OB02295A.

[6] D.A. Merkushev, S.D. Usoltsev, Y.S. Mar, A.P. Pushkarev, D. Volyniuk, J. V Grazulevicius, E. V Rumyantsev, BODIPY associates in organic matrices: Spectral properties, photostability and evaluation as OLED emitters, Mater. Chem. Phys. J. 187 (2017) 104–111. doi:10.1016/j.matchemphys.2016.11.053.

[7] A. Aguiar, J. Farinhas, M. Emilia, C.M.A. Brett, J. Morgado, A.J.F.N. Sobral, Synthesis, characterization and application of meso-substituted fluorinated boron dipyrromethenes (BODIPYs) with different styryl groups in organic photovoltaic cells, Dyes Pigment. 168 (2019) 103–110. doi:10.1016/j.dyepig.2019.04.031.

[8] K. Zhang, Z. Yang, B. Wang, S. Sun, Y. Li, T. Li, Z. Liu, J. An, A highly selective chemosensor for Al_3^+ based on 2-oxo-quinoline-3-carbaldehyde Schiff-base, Spectrochim. Acta Part A Mol. Biomol. Spectrosc. 124 (2014) 59–63. doi:10.1016/j.saa.2013.12.076.

[9] M. Tsuchikawa, A. Takao, T. Funaki, H. Sugihara, K. Ono, Multifunctional organic dyes: anion-sensing and light-harvesting properties of curcumin boron complexes, RSC Adv. 7 (2017) 36612–36616. doi:10.1039/C7RA06778J.

[10] Y.Y. Kang, H. Jung, G. Yu, Y. Chong, H. Mok, Complexation of curcumin with 2-aminoethyl diphenyl borate and implications for spatiotemporal fluorescence monitoring, Int. J. Pharm. 515 (2016) 669–676. doi:10.1016/j.ijpharm.2016.10.073.

[11] M. Pröhl, U.S. Schubert, W. Weigand, M. Gottschaldt, Metal complexes of curcumin and curcumin derivatives for molecular imaging and anticancer therapy, Coord. Chem. Rev. 307 (2016) 32–41. doi:10.1016/j.ccr.2015.09.001.

[12] S.N. Margar, N. Sekar, Red and near-infrared emitting bis-coumarin analogues based on curcumin framework-synthesis and photophysical studies, J. Photochem. Photobiol. A Chem. 327 (2016) 58–70. doi:10.1016/j.jphotochem.2016.05.009.

[13] B. Stefane, F. Pozgan, E. Kim, E. Choi, J. Ribierre, J. Weon, M. Ponce-vargas, B. Guennic, D. Jacquemin, G. Canard, E. Zaborova, F. Fages, A. D´Aléo, Ethynylene-analogues of hemicurcuminoids: Synthesis and ground-and excited properties of their boron difluoride complexes, Dye. Pigment. 141 (2017) 38–47. doi:10.1016/j.dyepig.2017.02.005.

[14] A. Chaicham, S. Kulchat, G. Tumcharern, T. Tuntulani, Synthesis, photophysical properties, and cyanide

detection in aqueous solution of BF_2-curcumin dyes, Tetrahedron. 66 (2010) 6217–6223. doi:10.1016/j.tet.2010.05.088.

[15] M.C. Mandewale, U.C. Patil, S. V Shedge, U.R. Dappadwad, R.S. Yamgar, A review on quinoline hydrazone derivatives as a new class of potent antitubercular and anticancer agents, Beni-Suef Univ. J. Basic Appl. Sci. 6 (2017) 354–361. doi:10.1016/j.bjbas.2017.07.005.

[16] X. Chu, C. Wang, W. Liu, L. Liang, K. Gong, C. Zhao, K. Sun, Quinoline and quinolone dimers and their biological activities: An overview, Eur. J. Med. Chem. 161 (2019) 101–117. doi:10.1016/j.ejmech.2018.10.035.

[17] M. Mao, X. Zhang, B. Zhu, J. Wang, G. Wu, Y. Yin, Q. Song, Comparative studies of organic dyes with a quinazoline or quinoline chromophore as Π-conjugated bridges for dye-sensitized solar cells, Dye. Pigment. 124 (2016) 72–81. doi:10.1016/j.dyepig.2015.09.002.

[18] M. Mao, J. Wang, X. Liu, G. Wu, X. Fang, Q. Song, Insight into the effects of modifying chromophores on the performance of quinoline-based dye-sensitized solar cells, Spectrochim. Acta Part A Mol. Biomol. Spectrosc. 190 (2018) 23–32. doi:10.1016/j.saa.2017.09.002.

[19] A. Slodek, D. Zych, A. Maro, S. Golba, E. Schab-Balcerzak, H. Janeczek, M. Siwy, S. Ma, Fluorene vs carbazole substituent at quinoline core toward organic electronics, Dye. Pigments. 166 (2019) 98–106. doi:10.1016/j.dyepig.2019.03.032.

[20] G. Paramaguru, R.V. Solomon, S. Jagadeeswari, P. Venuvanalingam, R. Renganathan, Tuning the photophysical properties of 2-quinolinone-based donor – Acceptor molecules through *N*- versus *O*-alkylation: insights from experimental and theoretical investigations, Eur. J. Org. Chem. (2014) 753–766. doi:10.1002/ejoc.201301085.

[21] P. Ganesan, A. Chandiran, P. Gao, R. Rajalingam, M. Gratzel, M.K. Nazeeruddin, Molecular engineering of 2-quinolinone based anchoring groups for dye-sensitized solar cells, J. Phys. Chem. 118 (2014) 16896−16903. doi:dx.doi.org/10.1021/jp5004352 |.

[22] K. Liu, J. Chen, J. Chojnacki, S. Zhang, BF_3.OEt_2-promoted concise synthesis of difluoroboron-derivatized curcumins from aldehydes and 2,4-pentanedione, Tetrahedron Lett. 54 (2013) 2070–2073. doi:10.1016/j.tetlet.2013.02.015.

[23] F. Payton, P. Sandusky, W.L. Alworth, NMR study of the solution structure of curcumin, J. Nat. Prod. 70 (2007) 4–7. doi:10.1021/np060263s.

[24] G. Bai, C. Yu, C. Cheng, E. Hao, Y. Wei, X. Mu, L. Jiao, Syntheses and photophysical properties of BF_2 complexes of curcumin analogues, Org. Biomol. Chem. 12 (2014) 1618-1626. doi10.1039/c3ob42201a

[25] M. Kasha, H.R. Rawls, A. El-Bayoumi, The exciton model in molecular spectroscopy, Pure Appl. Chem. 11 (1964) 371–392. doi:10.1351/pac196511030371.

[26] J. Lee, T. Joo, Photophysical model of 10-hydroxybenzo[*h*]quinoline: Internal conversion and excited state intramolecular proton transfer, Bull. Korean Chem. Soc. 35 (2014) 881-885. doi: 0.5012/bkcs.2014.35.3.881

[27] O.A. Kucherak, P. Didier, M. Yves, A.S. Klymchenko, Fluorene analogues of Prodan with superior fluorescence brightness and solvatochromism, J. Phys. Chem. Lett. 1 (2010) 616–620. doi:10.1021/jz9003685.

Credit Author Statement:

R.A.: Conceptualization, Supervision. **D.I**., **L.C.** and **A.O.:** Investigation, Methodology. **A.O.:** Formal analysis. **R.A., D.I**., **L.C.**, **A.O.**, **B.I.** and **J.Q.:** Writing - Original draft preparation, Visualization, Writing - Reviewing and Editing.

Declaration of interests

☒ The authors declare that they have no known competing financial interests or personal relationships that could have appeared to influence the work reported in this paper.

☒The authors declare the following financial interests/personal relationships which may be considered as potential competing interests:

None

Highlights

- The synthesis and characterization of two series of new *bis*-quinolin curcuminoid BF_2-complexes and their decomplexed derivatives is reported.
- Synthesized compounds displayed interesting optical properties.
- BF_2-complex and their decomplexed derivatives showed fluorescent properties both in solution and in solid state.
- Studies revealed that the absorption and emission bands for both series of compounds are dependent of their structures but also of the type of substituent.
- Experimental data were confirmed through computational calculations at DFT level via simulations of the Uv-vis spectra and determining the topology of the border orbitals responsible for light absorption.